

Observation of quasiperiodic dynamics in a one-dimensional quantum walk of single photons in space

Peng Xue^{*,1,2} Hao Qin,¹ Bao Tang,¹ and Barry C. Sanders^{3,4}

¹*Department of Physics, Southeast University, Nanjing 211189, China*

²*State Key Laboratory of Precision Spectroscopy,*

East China Normal University, Shanghai 200062, China

³*Hefei National Laboratory for Physical Sciences at Microscale and Department of Modern Physics, University of Science and Technology of China, Hefei, 230026, China*

⁴*Institute for Quantum Science and Technology, University of Calgary, Alberta T2N 1N4, Canada*

We realize quasi-periodic dynamics of a quantum walker over 2.5 quasi-periods by realizing the walker as a single photon passing through a quantum-walk optical-interferometer network. We introduce fully controllable polarization-independent phase shifters in each optical path to realize arbitrary site-dependent phase shifts, and we employ large clear-aperture beam displacers, while maintaining high-visibility interference, to enable reaching 10 quantum-walk steps. By varying the half-wave-plate setting, we control the quantum-coin bias thereby observing a transition from quasi-periodic dynamics to ballistic diffusion.

PACS numbers: 03.65.Yz, 05.40.Fb, 42.50.Xa, 71.55.Jv

The quantum walk (QW) [1, 2] is a quantized version of the ubiquitous random walk (RW) used for describing diffusion [3], for probabilistic algorithms [4] to solve constraint satisfaction problems in computer science [5], for quantum transport in complex systems [6] and for demonstrating intriguing nonlinear dynamical quantum phenomena [7]. In its basic formulation a walker moves on an integer lattice with its periodic spatial sites labelled by integers x . This one-dimensional line is regarded as being arbitrarily long and the walker commences at the origin $x = 0$. The walker carries a two-sided coin with the two sides labelled by $c \in \{0, 1\}$.

The walker's evolution proceeds as follows: the walker flips the coin to obtain an outcome c and then makes one step in the positive or negative direction on the line if the coin flip yields the outcome 0 or 1, respectively. The randomness of the coin flip leads to a diffusion rate that increases as \sqrt{t} with t the time of evolution (which we treat as a non-negative integer incrementing by one unit per step from $t = 0$); this square-root dependence is characteristic of diffusive spreading, with "spread" signifying the width of the position distribution $P_t(x)$ at time t .

The QW eliminates random evolution by trading the coin for a quantum two-level system, which, in our case, is the polarization state of a single photon: horizontal (H) or vertical (V). Furthermore the QW employs unitary dynamics by which the walker's position is entangled with the coin state. When the evolution is complete, the coin state is ignored, which mathematically corresponds to tracing out this degree of freedom.

For this evolution, the walker's position distribution then spreads proportional to t rather than to \sqrt{t} . Pro-

portionality of position spreading to t is reminiscent of constant-velocity deterministic motion and is thus known as "ballistic transport". QWs are widely studied experimentally and theoretically because of their applications to quantum algorithms [3] and quantum transport [6] and also for intriguing foundational studies of quantum phenomena such as defect-induced localization [8, 9] and quantum resonances [10, 11].

Mathematically each evolutionary "step" given by unitary operator U on the joint walker-coin system is achieved by repeating two sequential unitary operations. The first operation is the unitary analogue of the coin flip achieved by transforming the coin states $|c = 0\rangle$ and $|c = 1\rangle$ to $\cos\theta|0\rangle + \sin\theta|1\rangle$ and $\sin\theta|0\rangle - \cos\theta|1\rangle$, respectively, with θ the coin-bias parameter. The second (entangling) operation translates the walker's position dependent on the coin state: $\sum_{c=0}^1 \sum_{x=-\infty}^{\infty} e^{i\phi(x)} |x + (-1)^c\rangle \langle x| \otimes |c\rangle \langle c|$. Typically $\phi(x) \equiv 0$ in theory [12–16] and experiment [17–25], but controllably varying the phase enables the realizations of remarkable quantum-walk properties such as quantum recurrences in diffusion, which arise in the "harmonic case" $\phi(x) = 2\pi xy$ for $y = q/p$; we focus on q, p co-prime integers [7].

The walker is manifested experimentally as a single photon and the lattice as a set of allowed paths for the photon. Pairs of 800nm photons are generated via type-I spontaneous parametric down conversion (SPDC) in two 0.5mm-thick nonlinear- β -barium-borate (BBO) crystals cut at 29.41° , which are pumped by a 100mW 400nm continuous-wave diode laser. Triggering on one photon prepares the other photon in the pair as a single-photon state. After spectral filtering with full-width-at-half-maximum (FWHM) 3nm, individual down-converted photons are steered into the optical modes of the linear-optical network formed by a series of birefringent calcite beam displacers (BDs), half-wave

*gnep.eux@gmail.com

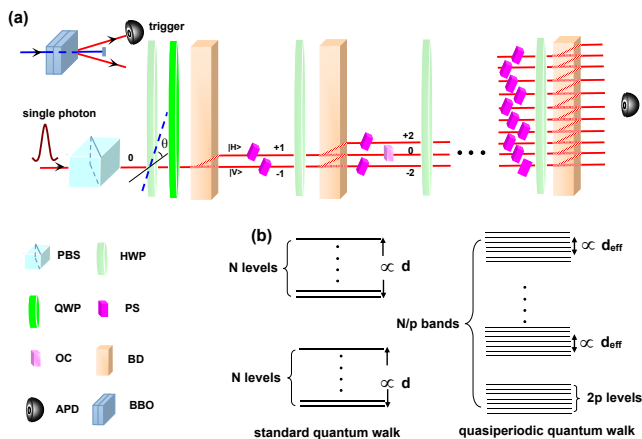


FIG. 1: Experimental scheme for 10-step QW with position-dependent phase function. (a) Single-photons are created via spontaneous parametric down conversion in two β -Barium Borate (BBO) crystals. One photon in the pair is detected to herald the other photon, which is injected into the optical network. Arbitrary initial coin states are prepared by a polarizing beam splitter (PBS) and half-wave plates (HWP) and quarter-wave plates (QWP). Phase shifters (PS) are placed in separate transverse spatial modes, and optical compensators (OC) compensate their resultant temporal delays. Coincident detection of trigger and heralded photons at avalanche photodiodes (APDs) yields data for the QW. (b) Quasi-energy spectra for the standard and quasi-periodic QW respectively.

plates (HWPs) and phase shifters (PSs). Output photons are detected using avalanche photo-diodes (APDs, 7ns time window) with a dark count rate of less than 100s^{-1} whose coincident signals—monitored using a commercially available counting logic—are used to postselect two single-photon events. The total coincident counts are around 20,000 over 40s. The probability of creating more than one photon pair is less than 10^{-4} and can thus be neglected.

Optical interferometers comprising birefringent-crystal BDs, wave plates (WPs), and PSs serve as stable devices for simulating quantum information processes such as heralded coined QWs. The interferometer set-up is shown in Fig. 1(a). The 10-step QW is implemented with a single HWP, BD, and PSs in each path signifying one possible site for the walker. The coin state corresponds to the polarization of the photon, which is produced by SPDC creating correlated photons pairs at random times. One photon in the pair is the signal photon, which undergoes the QW, and the other is the trigger photon, which heralds the presence of the signal photon. Experimentally QW dynamics is detected by photon coincidence measurements between the signal and the trigger photon.

Ten BDs, each with length 28.165mm and a clear aperture of $33\text{mm} \times 15\text{mm}$, are placed in sequence and need to have their optical axes mutually aligned. Co-alignment ensures that beams split by one BD in the sequence yield

maximum interference visibility after passing through a HWP and the next BD in the sequence. In our experiment, we attain interference visibility of 0.998 for each step, i.e., for each pair of sequential BDs.

Output photons from the interferometric network are coupled into a single-mode optical fibre and subsequently detected by an APD in coincidence with the trigger photon. We characterize the quality of the experimental QW by its 1-norm distance [2] from the simulated QW according to $\frac{1}{2} \sum_x |P^{\text{exp}}(x) - P^{\text{th}}(x)|$; in our case this distance is 0.085 after 10 steps. The distance increases monotonically with each step number due to a lack of relative phase control between the multiple interferometers. This limited control is due to nonplanar optical surfaces. By placing 10 crystals in sequence, we are able to achieve 10 quantum-walk steps, surpassing the previous limit of 7 quantum-walk steps in a similar interferometric set-up [25].

The symmetric initial coin state $(|0\rangle + i|1\rangle)/\sqrt{2}$ ensures a symmetric walker position distribution and is prepared by sending the signal photon through a polarizing beam splitter followed by a HWP and subsequently by a quarter-wave plate (QWP). A birefringent BD steers a photon to two possible pathways 3mm apart in a polarization-dependent way, which effects the coin-state-dependent walker translation but without incorporating the position-dependent phase function.

We introduce a PS in every path between every pair of BDs and thereby obtain full phase-controlled coin-state-dependent walker translation. Microscope slides (MSs) with certain effective thickness are introduced as PSs into the interferometric network after first completing the alignment described above and ensuring maximum interference and small distance between simulated and empirical walker distributions. The MSs are inserted and aligned to recover the case of zero phase shift $\phi(x) = 0$ for all locations x . This microscope-slide alignment corresponds to each slide being in the plane perpendicular to the beams in each path.

After achieving this alignment, each MS can be adjusted to an effective thickness in order impart a controllable phase shift independent of all other PSs. This effective thickness is achieved by rotating the slide out of the plane perpendicular to the beams. Tilting the slide is a viable alternative but is not as stable for the times required to gather the data.

As an example, we explain how to align the slides for the second quantum-walk step. In this case there are two PSs because there are two longitudinal spatial modes after the first step. We rotate the two PSs separately, then gather photon-count data. These data are compared to the theoretical simulation. If the data are not satisfactory with respect to the 1-norm distance of the walker distribution, we discard the data, adjust the PSs and repeat. When the data agree well with the theory, we retain the walker distribution results and then add the third step of

the walker by adding another three PSs within the three longitudinal spatial modes respectively, a HWP and BD and repeat this procedure.

Our chief technical innovation in addition to reaching 10 steps is the development of fully controllable polarization-independent PSs that can be inserted into each optical path of a quantum-walk interferometer. These controllable PSs greatly increase the versatility of quantum-walk optical-interferometer networks as they enable generalized QWs with arbitrary phase functions $\phi(x)$. We insert PSs into each optical path and adaptively calibrate and adjust the phases through sequential tests until the alignments achieve the desired $\phi(x)$ within acceptable tolerances.

The effectiveness of these controllable PSs is demonstrated by realizing here quasi-periodic dynamics in a QW for the first time. Our quasi-periodic evolution has been achieved over 2.5 quasi-periods, which suffices to see an unambiguous experimental signature revealing the quasi-period.

Quasi-periodic dynamics arises through symmetry breaking due to the imposition of the position-dependent phase shift. This position-dependent phase shift leads to an effective periodic potential. For q co-prime to p , the potential wells behave effectively as a family of N/p clusters, and we henceforth let p be even. For the quasi-energy spectrum being the argument of the eigenvalues of U , the clustering of wells leads to quasi-energy bands comprising $2p$ quasi-energy levels each of which only one is doubly degenerate.

We show the quasi-energy spectra in Fig. 1(b) for $y = q/p$ with the standard quantum-walk case $q = 0$ shown on the left and the $q \neq 0$ case depicted on the right. Since we use two-side coin we have two bands of Bloch levels, each consisting of N spectral lines which are equally spaced for $q = 0$, and the width of each band proportional to the tunneling amplitude $d = \cos\theta$. On the other hand, for even p and $q \neq 0$, spectral lines collect into p Bloch bands with $2p - 1$ lines per band and the bandwidth is proportional to the effective tunneling amplitude $d_{\text{eff}} := d^{p/2}$. Hence U^p is close to the identity thereby ensuring a quasi-revival of the initial state after every p steps [7].

The quasi-energies $E_{\ell mn}$ of the quantum walker navigating a lattice with position-dependent phase shifts are given by $\arg(\lambda_{\ell mn})$ with $\lambda_{\ell mn}$ the eigenvalues of the unitary operator U and $\ell = 0, 1, \dots, N/p - 1$, $m = 0, 1$, and $n = 0, 1, \dots, p - 1$ [7]. For even p , the eigenvalues are [7]

$$\lambda_{\ell mn} = e^{2\pi \frac{in}{p}} \left(2ir_{\ell} \left[(-1)^m \sqrt{1 - r_{\ell}^2} - ir_{\ell} \right]^{1/p} - 1 \right),$$

for $r_{\ell} = d^{p/2} \sin(\pi p \ell / N)$.

A degeneracy emerges for even p , i.e., for $E_{\ell mn}$ with $n \geq p - 1$ are same. Therefore, there are a total of p quasi-energy bands, each consisting of $2p$ levels with two of them, namely E_{000} and E_{010} , being degenerate. For

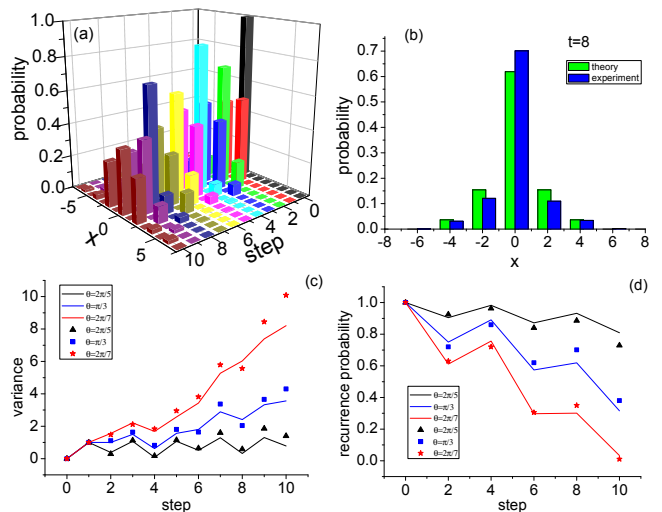


FIG. 2: Quasi-periodicity of the QW. (a) Experimental position distributions for successive steps of the $C(\pi/3)$ coined QW with position-dependent phase function $\phi(x) = 2\pi x/4$ and a symmetric initial coin state up to 10 steps. (b) Probability distribution of the 8-step QW evolved after two quasi-periods ($t = 8$). Blue and green bars show experimental data and theoretical predictions respectively. (c) Measured position variance and (d) recurrence probability of quasi-periodic QW with various coin operations $C(2\pi/5)$ (black triangles), $C(\pi/3)$ (blue boxes) and $C(2\pi/7)$ (red stars) for 1 to 10 steps, compared to theoretical predictions (solid lines). Error bars are smaller than symbol size.

example, in our case with $p = 4$, the resulting system has 4 energy bands, each band comprising 7 quasi-energy levels, and the width of the band is proportional to d^2 .

For d small, the bands are narrow, and the system is nearly harmonic: quasi-periodic dynamics is expected. For d large, non-harmonic effects should emerge, and consequently a transition from quasi-periodic behaviour to ballistic spreading is expected.

We can see the quasi-periodicity arising in our theoretical simulation and from the experimental data depicted in Fig. 2 for $y = 1/4$, i.e., by setting $q = 1$ and $p = 4$. In Fig. 2(a), we see the experimental data for the walker distribution at each step $t = 0, 1, 2, \dots, 10$ with $\theta = \pi/3$. The distribution narrows almost to the initial spike at $x = 0$ for $t = 4$ and $t = 8$ but has additional support for $x \neq 0$; i.e., width of the position distribution has increased. In contrast, for the standard QW corresponding to any integer-valued y , the probability distribution spreads monotonically with a width proportional to t as seen in the previous 6-step standard-quantum-walk experiment [2].

Theoretical vs. experimental results are shown in Fig. 2(b) for $t = 8$, which shows their close agreement and also the degree of spreading after two periods of quasi-periodic revival of the position distribution. Figures 2(a,b) suggest a quasi-periodic revival of the position

distribution with period $\tau = 4$, and Figs. 2(c,d) enable quantitative analysis to determine τ for various values of θ . The variance and recurrence probability $P_t(x=0)$ are shown in Figs. 2(c,d), respectively. Each plot shows an unambiguous period of $\tau = 4$ as expected from our choice of $p = 4$, thereby confirming our numerical simulation and our experiment.

The coin bias θ enables tuning between two extremal modes of behaviour. One extremal mode is the adiabatic limit corresponding to a truly periodically varying walker position distribution with a tendency of trapping at the origin. At the other extreme we have the diabatic limit of no recurrences with just the standard QW with ballistic spreading being manifested. The coin bias is a convenient and effective control of diabaticity vs adiabaticity because θ can set the rate for position spreading without modifying the nature of the position distribution.

Experimentally the coin bias is controlled by adjusting the angle of a HWP, and experimental results for the walker's position distribution are shown in Fig. 3(a) at the first quasi-period $t = 4$ for various choices of θ . Increased narrowing of the distribution for increased θ is commensurate with the expected transition from diabatic to adiabatic behaviour. The time-dependent variance for theory and experiment for various θ in Fig. 3(b) further confirm the diabatic-to-adiabatic transition especially showing the vanishing of quasi-periodicity in the diabatic limit, yielding instead ballistic spreading.

Now that we have established that our experiment shows quasi-periodic dynamics and a full transition from adiabatic to diabatic behaviour by controlling the coin bias, we proceed to show the quantum-to-classical transition from quasi-periodic to diffusive dynamics through controlling decoherence in the optical interferometer network. This decoherence is controlled by tilting BDs, as shown in Fig. 4(a), leads to a spatiotemporal mode mismatch. This mismatch leads to dephasing between the relative paths and therefore manifests decoherence of the QW.

We choose $\Delta\theta = 9.75^\circ$ to realize full decoherence of the QW [2] and show in Figs. 4(b, c, d) the results for the walker position distribution and normalized variance in the coherent and decoherent cases for $t = 4$. Thus, we can see the dramatic transition from quasi-periodic dynamics to ordinary diffusive dynamics through controlled decoherence on the scale of one quasi-period.

In summary we have developed a versatile optical quantum network with single-photon inputs that can simulate QWs with arbitrary position-dependent phase shifts. We show quasi-periodic dynamics of a quantum walker and clear signatures of adiabatic vs diabatic behaviour as well as quasi-periodic-to-diffusive dynamics by controlling decoherence. Our results show a new realm of quantum-walk phenomenon which is especially interesting in the context of quantum chaos and Bloch os-

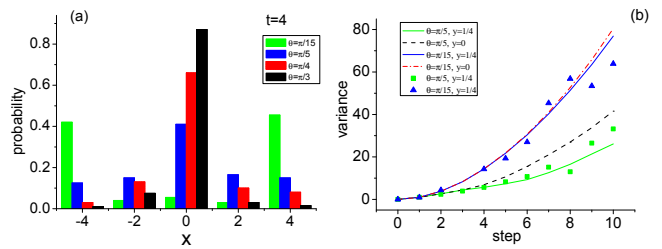


FIG. 3: Adiabatic to diabatic transition of the QW. Transition for various coin-flip biases, position-dependent phase function $\phi(x) = 2\pi x/4$ and a symmetric initial coin state. (a) Experimental position distributions after the first quasi-period τ . (b) Measured and predicted variances for 10 steps compared to a standard QW simulation with $\phi(x) \equiv 0$. Error bars are smaller than symbol size.

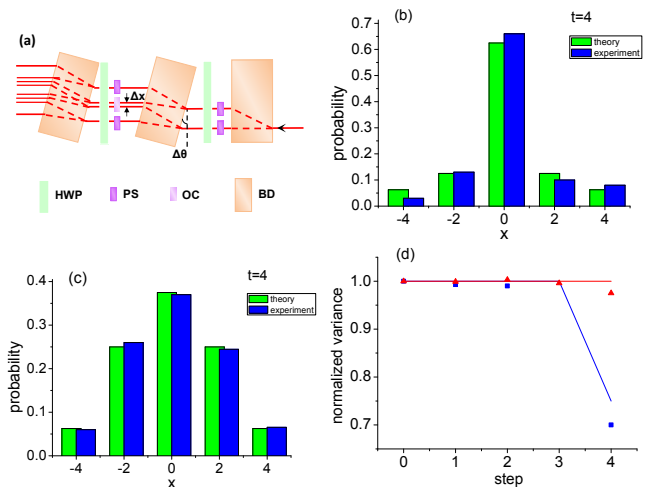


FIG. 4: Transition from quasi-periodic QW to fully decohered QW. (a) A relative angle $\Delta\theta$ between two beam displacers reduces the recombined photon's spatial mode overlap, which introduces controllable dephasing. (b) Measured position distribution at the first quasi-period with coin bias $\theta = \pi/4$, position-dependent phase function $\phi(x) = 2\pi x/4$ and a symmetric initial coin state. (c) Position distribution of a fully decohered QW. Blue and green bars show experimental data and theoretical predictions respectively. (d) Normalized position variances of quasi-periodic QW (blue boxes) and of fully decohered QW (red triangles) up to 4 steps, compared to theoretical predictions (solid lines). Error bars are smaller than symbol size.

cillations and our new interferometer phase-shift control provides a valuable new tool for exploring QWs with various potentials.

We acknowledge experimental guidance from Xiao-Ye Xu, Kai Sun, Jin-Shi Xu, Chuan-Feng Li and Guang-Can Guo. This work has been supported by NSFC under 11004029 and 11174052, NSFJS under BK2010422, 973 Program under 2011CB921203, the Open Fund from the State Key Laboratory of Precision Spectroscopy of East China Normal University, the 1000 Talent Program of

China, the Canadian Institute for Advanced Research, and Alberta Innovates Technology Futures.

-
- [1] D. Bouwmeester, I. Marzoli, G. P. Karman, W. Schleich, and J. P. Woerdman, *Phys. Rev. A* **61**, 013410 (1999).
- [2] M. A. Broome, A. Fedrizzi, B. P. Lanyon, I. Kassal, A. Aspuru-Guzik, and A. G. White, *Phys. Rev. Lett.* **104**, 153602 (2010).
- [3] A. M. Childs, R. Cleve, E. Deotto, E. Farhi, S. Gutmann, and D. A. Spielman, *Proc. 35th ACM Symposium on Theory of Computing (STOC 2003)*, pp. 59-68.
- [4] A. M. Childs, R. Cleve, E. Deotto, E. Farhi, S. Gutmann, and D. A. Spielman, *Proc. 35th ACM Symposium on Theory of Computing (STOC 2003)*, pp. 59-68.
- [5] U. Schöning, *Proceedings of the 40th Annual IEEE Symposium on Foundations of Computer Science, FOCS'99* 410–414 (1999).
- [6] A. C. Oliveira, R. Portugal, and R. Donangelo, *Phys. Rev. A* **74**, 012312 (2006).
- [7] A. Wójcik, T. Łuczak, P. Kurzyński, A. Grudka, and M. Bednarska, *Phys. Rev. Lett.* **93**, 180601 (2004).
- [8] A. Crespi, R. Osellame, R. Ramponi, V. Giovannetti, R. Fazio, L. Sansoni, F. De Nicola, F. Sciarrino, and P. Mataloni, *Nat. Photo.* **7**, 322-328 (2013).
- [9] A. Schreiber, K. N. Cassemiro, V. Potoček, A. Gábris, I. Jex, and Ch. Silberhorn, *Phys. Rev. Lett.* **106**, 180403 (2011).
- [10] M. Genske, W. Alt, A. Steffen, A. H. Werner, R. F. Werner, D. Meschede, and A. Alberti, *Phys. Rev. Lett.* **110**, 190601 (2013).
- [11] C. Cedzich, T. Rybár, A. H. Werner, A. Alberti, M. Genske, R. F. Werner, *Phys. Rev. Lett.* **111**, 160601 (2013).
- [12] N. Shenvi, J. Kempe, and K. B. Whaley, *Phys. Rev. A* **67**, 052307 (2003).
- [13] T. A. Brun, H. A. Carteret, and A. Ambainis, *Phys. Rev. Lett.* **91**, 130602 (2003).
- [14] T. Kitagawa, M. S. Rudner, E. Berg, and E. Demler, *Phys. Rev. A* **82**, 033429 (2010).
- [15] R. Côté, A. Russell, E. E. Eyler, and P. L. Gould, *New J. Phys.* **8**, 156 (2006).
- [16] M. C. Bañuls, C. Navarrete, A. Pérez, E. Roldán, and J. C. Soriano, *Phys. Rev. A* **73**, 062304 (2006).
- [17] M. Karski, L. Forster, J. M. Choi, A. Steffen, W. Alt, D. Meschede, and A. Widera, *Science* **325**, 174 (2009).
- [18] A. Peruzzo, M. Lobino, J. C. F. Matthews, N. Matsuda, A. Politi, K. Poulios, X. Zhou, Y. Lahini, N. Ismail, K. Worhoff, Y. Bromberg, Y. Silberberg, M. G. Thompson, and J. L. O'Brien, *Science* **329**, 1500 (2010).
- [19] H. B. Perets, Y. Lahini, F. Pozzi, M. Sorel, R. Morandotti, and Y. Silberberg, *Phys. Rev. Lett.* **100**, 170506 (2008).
- [20] A. Schreiber, A. Gábris, P. P. Rohde, K. Laiho, M. Štefaňák, V. Potoček, C. Hamilton, I. Jex, and C. Silberhorn, *Science* **336**, 55 (2012).
- [21] A. Schreiber, K. N. Cassemiro, V. Potoček, A. Gábris, P. J. Mosley, E. Andersson, I. Jex, and Ch. Silberhorn, *Phys. Rev. Lett.* **104**, 050502 (2010).
- [22] L. Sansoni, F. Sciarrino, G. Vallone, P. Mataloni, A. Crespi, R. Ramponi, and R. Osellame, *Phys. Rev. Lett.* **108**, 010502 (2012).
- [23] B. Do, M. L. Stohler, S. Balasubramanian, D. S. Elliott, C. Eash, E. Fischbach, M. A. Fischbach, A. Mills, and B. Zwickl, *J. Opt. Soc. Am. B* **22**, 499 (2005).
- [24] P. Zhang, X. F. Ren, X. B. Zou, B. H. Liu, Y. F. Huang, and G. C. Guo, *Phys. Rev. A* **75**, 052310 (2007).
- [25] T. Kitagawa, M. A. Broome, A. Fedrizzi, M. S. Rudner, E. Berg, I. Kassal, A. Aspuru-Guzik, E. Demler, and A. G. White, *Nat. Commun.* **3**, 882 (2012).